J Mater Sci (2020) 55:10833–10848

Metals & corrosion

Intergranular corrosion behavior of extruded 6005A alloy profile with different microstructures

Chengxiong Duan[1], Jianguo Tang[1,2], Wenjing Ma[1], Lingying Ye[1], Haichun Jiang[3,*], Yunlai Deng[1,2], and Xinming Zhang[1,2]

[1] School of Materials Science and Engineering, Central South University, Changsha 410083, China
[2] Collaborative Innovation Center of Advanced Nonferrous Structural Materials and Manufacturing, Central South University, Changsha 410083, China
[3] Zhejiang Mintai Technology Co., Ltd. and MINTH Research and Development Center, Huzhou 313300, China

Received: 11 December 2019
Accepted: 15 April 2020
Published online: 4 May 2020

ABSTRACT

The intergranular corrosion (IGC) behavior of an extruded 6005A alloy profile with the coexisting of peripheral coarse grain (PCG) structure and partial recrystallized grain (PRG) structure was investigated by using an accelerated corrosion test, electrochemical impedance spectroscopy and a quasi in situ examination of IGC process. PCG structure was found to have a unique IGC behavior that pitting corrosion and subsequent IGC are less severe and will not be transformed into intragranular corrosion as they were found in PRG structure. Microstructure characterization reveals that the microstructural differences in grain boundary precipitates, primary α-AlFeMnSi intermetallic particles and grain characteristic between PCG structure and PRG structure are the reason for these phenomena. Further analysis indicates that the grain boundaries decorated with more AlFeMnSi particles and Q phase precipitates are more sensitive to corrosion, where Q phase precipitates are the primary cathodes and the most important factor affecting IGC; AlFeMnSi particles are supposed to initiate pitting corrosion since they are dissolved as anodes in the early stage of corrosion. With the development of corrosion, they are transformed into cathodes and become the bridges of IGC propagation by connecting the Q phase precipitates at grain boundary. In addition, grain characteristic was also found to have great effects on IGC. With the decrease in grain size and the increase in the frequency of high-angle grain boundaries and the dislocation density, corrosion becomes more severe and more likely to be transformed into intragranular corrosion.

Address correspondence to E-mail: haichun.jiang@minthgroup.com

https://doi.org/10.1007/s10853-020-04692-6

Introduction

6xxx alloys (Al–Mg–Si–(Cu)) are widely used in transport and other market sectors because of their superior comprehensive properties including medium strength, low density, good corrosion resistance, weldability and formability [1]. However, 6xxx alloys still suffer from intergranular corrosion (IGC) if they are improperly heat treated and/or alloyed [2–9], for example long-time overaging in alloys with high content of Cu and excessive Si. IGC results from the presence of the electrochemically active paths along grain boundaries, which consist of grain boundary precipitates, Al matrix and precipitation free zones (PFZs), and usually takes place together with other kinds of localized corrosion. It is reported that IGC and pitting corrosion can be transformed from one to the other [10–12] and were found to propagate into the interior, which is referred to as intragranular corrosion, of the grains with high dislocation density [13–18] and/or specific crystallographic orientations [12]. Therefore, the investigation of the IGC behavior of aluminum alloy should take pitting corrosion, intragranular corrosion and IGC into consideration, which makes investigation more complicated.

The IGC of 6xxx alloys has been investigated for many years, and some commonly accepted conclusions are listed as follows. With the addition of Cu into 6xxx alloys, a part of grain boundary precipitates can be transformed from β-phase precipitates into Cu-containing precipitates (Q phase, θ phase or S phase) [19–21]. Meanwhile, grain boundary Cu film can also be found in Al–Mg–Si–Cu alloys, which is supposed to be the precursor of Q phase precipitates [2, 22–25]. Generally, such Cu film is only capable of being resolved by 3D atom probe tomography (3D APT) or through STEM (if the grain boundaries are parallel to the electron beam) [22, 23]. The corrosion potential of Cu film and Cu-containing precipitates is far different from those of aluminum matrix and PFZs [3, 22, 23], and hence, the IGC resistance of 6xxx alloys decreases dramatically with the addition of Cu. The Si precipitates formed at grain boundary are usually found in Al–Mg–Si alloy with excessive Si, which will cause a severe anodic dissolution of aluminum matrix [8] and a change of fracture mode from plastic fracture to brittle fracture [26]. Fe is an impurity element in Al–Mg–Si alloys, and it forms several kinds of Fe-containing intermetallic particles (AlFe, AlFeSi, AlFeMnSi, etc.) by consuming Al, Si, Mn and Cu. Most reports claimed that Fe-containing particles are cathodically active and act as the initiation sites of pitting corrosion [27–29], and a few reports mentioned that the Fe-containing particles presenting at grain boundary form continuous IGC channels by connecting with Cu-containing particles [7]. However, the dissolution of such particles was also reported in the IGC of 6005A alloy [30]. This issue is important for investigating the IGC behavior of industrially pr"oduced aluminum alloys since they usually contain a relatively high concentration of Fe. On the other hand, the IGC behavior of 6xxx alloys is significantly affected by heat treatment as well and this effect is correlated to the chemical composition and the processing of alloys. Generally speaking, for Al–Mg–Si–Cu alloys, the peak-aged are the most susceptible to IGC due to the most continuous distribution of grain boundary precipitates. With the increase in aging time, the IGC susceptibility of alloys decreases gradually with the coarsening of grain boundary precipitates [2–4, 6, 7, 24, 25]. However, in heavily overaged alloys, the continuous distribution of grain boundary precipitates can be restored and extremely broad precipitation free zones (PFZs) are formed, both of which are detrimental for the IGC resistance of alloys [31]. Therefore, it can be summarized that the IGC resistance of alloys is related to the grain boundary microstructure and especially the property of the grain boundary precipitates.

Peripheral coarse grain (PCG) structure, a unique grain structure which is originated from the surface recrystallization caused by the inhomogeneous deformation during the extrusion process, is often regarded as a kind of surface defect due to its detrimental effects on the mechanical properties and the surface appearance of the extrudates [32]. It was once reported that the surface layer (PCG structure) of the extruded 6061 aluminum alloy would be heavily corroded by IGC [33]. However, recent investigations revealed that the PCG structure in Al–Mg–Si–Cu and Al–Zn–Mg alloys was more resistant to IGC than other structures [34–36]. As mentioned previously, there are many factors, such as dislocation density, grain boundary precipitates and crystallographic orientation, that would affect the IGC behavior of 6xxx alloys, and hence, there is no generally accepted mechanism about the effect of PCG structure on IGC behavior in studies. In addition, the great differences in the grain characteristic and the dispersoids between PCG structure and other structures would

further increase the difficulty in understanding the effect of PCG structure on IGC behavior.

In the present paper, the specimen with PCG structure and PRG structure was carefully cut from an extruded 6005A alloy profile for investigation. Therefore, the IGC behavior of PCG structure and partially recrystallized grain (PRG) structure can be investigated by using an accelerated corrosion test, electrochemical impedance spectroscopy (EIS) and a quasi in situ examination of IGC process. And a detailed microstructure characterization including scanning electron microscope (SEM), electron backscattering diffraction (EBSD) and scanning transmission electron microscopy (STEM) were used to reveal the underlying mechanism about those different IGC behaviors and hence to deepen the understanding of the IGC behavior of 6xxx alloys.

Experiments

Materials and pretreatment

An industrially produced extruded 6005A alloy (Si 0.76 wt%, Fe 0.21 wt%, Cu 0.09 wt%, Mn 0.43 wt%, Mg 0.62 wt%, Cr 0.10 wt%, Al rem.) profile in T5 temper was used in the present paper, which was extruded, on-line quenched and artificially aged at 170 °C for 8 h. As shown in Fig. 1, the metallographic structure of the extruded profile in as-received condition was examined in polarized light with an Olympus BX51M optical microscope (OM). Before OM examination, specimens were mechanically ground with silicon carbide (SiC) papers up to grade 1500 and polished with 2.5 μm diamond pastes and then anodized for 40 s with a solution of 195 mL distilled water and 5 mL HBF_4 at a voltage of 25 V.

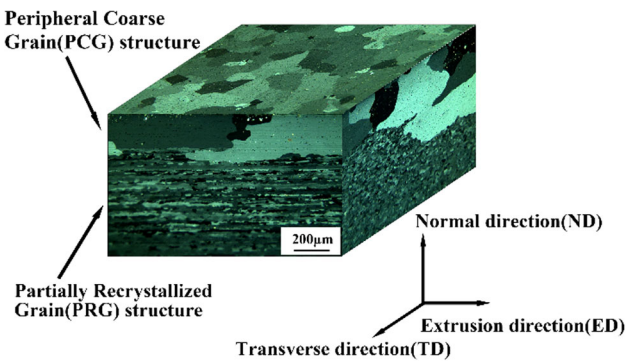

Figure 1 Optical micrographs of the as-received extruded profile.

According to the OM examination results, the maximum thickness of the PCG structure on single side of the extruded profile was 598.6 μm and its average thickness was more than 200 μm. In order to compare the IGC behavior and the microstructure of PCG structure and PRG structure, one half of extruded profile with the original surface containing PCG structure was denoted as PCG specimen and the other half with the PCG structure being completely removed by machining along the ED-TD plane was denoted as PRG specimen. All the specimens used in subsequent experiments were taken from these two groups.

Accelerated corrosion test

An accelerated corrosion test according to the method B of British standard ISO 11846: 2008 was used to investigate the IGC behavior of PCG specimen and PRG specimen. Specimens with a size of 15 mm × 10 mm × 2.5 mm were cut from the extruded profile. The lengthwise direction of the specimens is parallel to the extrusion direction of the extruded profile. To remove the original surface layer of specimens, specimens were degreased in ethanol and then etched in 10% NaOH solution for 5 min and desmuted in 30% HNO_3 solution for a few minutes. Before testing, all the surfaces, except the test surfaces, of specimens were covered by sealing glue and then specimens were immersed in an acidified sodium chloride solution of 30 g/L NaCl and 10 ml/L HCl for 24 h. Solution volume was 150 mL, and its temperature was maintained at 35 °C. After being immersed for 24 h, specimens were taken out from the solution, then rinsed with distilled water and dried. After that, specimens were cut to expose their cross sections which were then mechanically polished and examined with an OM and a Zeiss EVO MA10 scanning electron microscope (SEM). The propagation path of IGC was also characterized by EBSD analysis.

Quasi in situ examination of IGC process

The quasi in situ examination of IGC process was achieved by examining the surface morphological change of the fixed area on specimens with a SEM after specimens had been immersed in an acidified sodium chloride solution for different time. Its experimental procedure is almost same to that of the

accelerated corrosion test except that the test surfaces of specimens were mechanically polished rather than being cleaned by NaOH solution and HNO_3 solution before each corrosion of the fixed area, which was marked by a Vickers hardness indentations, of the test surfaces. To ensure that specimens are conductive in SEM observation, the opposite surfaces of the test surfaces were not covered by sealing glue and hence the volume of the acidified sodium chloride solution used in this experiment was 300 mL. After being immersed for some time (in this experiment, it was 0 h, 0.5 h, 2 h, 6 h), the surface morphologies of the fixed area were examined and hence a series of the SEM micrographs which shows the surface morphological change of the fixed area was obtained. After being immersed for 24 h in total, the surface morphologies of specimens were examined with a SEM to reveal the final corrosion performance of PCG specimens and PRG specimens.

EIS measurement

EIS measurement was carried out at open-circuit potential with a Multi Autolab/M204 electrochemical workstation and a three-electrode cell which consisted of a saturated calomel electrode (SCE) as a reference electrode, a platinum plate as a counter electrode and a specimen with a working area of 1 cm × 1 cm as a working electrode. Prior to measurement, specimens were ground with SiC papers up to grade 1500 and then mechanically polished, cleaned in ethanol and immersed in a naturally aerated acidified sodium chloride solution. After the open-circuit potential of specimens was stable, a signal with a frequency ranging from 10 kHz to 10 mHz and a 10 mV amplitude was applied on specimens and the corresponding data at each frequency were recorded. ZSimpWin software was employed for data modeling and curves fitting. The parameters obtained from software were used to evaluate the corrosion resistance of specimens, and the model of fitted curves was used to show the corrosion mechanism of specimens.

Microstructure characterization

SEM was used to measure the size, area fraction and the distribution of the second-phase particles in specimens, and the composition of those particles was semi-quantitatively analyzed with an energy-disperse spectrometer (EDS). EBSD data were used to analyze the grain characteristic including grain size, misorientation of grain boundaries and dislocation density. The dislocation density of specimens was calculated from EBSD data with a MATLAB toolbox, MTEX, developed by R. Hielscher. In EBSD maps, low-angle grain boundaries (LAGBs) with a misorientation angle within the range of 5°–15° are represented by thin black lines and high-angle grain boundaries (HAGBs) with a misorientation angle more than 15° are represented by thick black lines. The specimens for EBSD analysis were electro-polished in a solution of 10 mL $HClO_4$ and 90 mL ethanol for 5 s with a voltage of 20 V to remove surface stress layer after they had been mechanically polished.

The grain boundary precipitates of specimens were characterized with the STEM mode of the Titan G1 60-300 spherical aberration-corrected transmission electron microscope operated at 200 kV. The compositional information of precipitates was obtained by using an EDS. To prepare STEM specimens, thin foils cut from the surface and the middle of the extruded profile were mechanically thinned to 80 μm and were punched into Φ3 mm discs and then electro-polished in a electrolyte of 30 vol% nitric acid and 70 vol% methanol at about − 20 °C with a RL-2 electro-polisher.

Results

IGC behavior of extruded 6005A alloy profile

Accelerated corrosion test

The cross-sectional corrosion morphologies of the specimens after accelerated corrosion test are shown in Fig. 2a, b. In both PCG specimen and PRG specimen, network-shaped IGC cracks were found and some cracks are connected to surface corrosion pits. However, the morphology of the IGC cracks in PCG specimen is much different from that in PRG specimen. The IGC cracks in PCG specimen are usually straight with few branches, but the IGC cracks in PRG specimen are more twisted and tangled up with each other. The maximum depth, average depth and the maximum width of the IGC cracks in both specimens were measured with an OM and are shown in

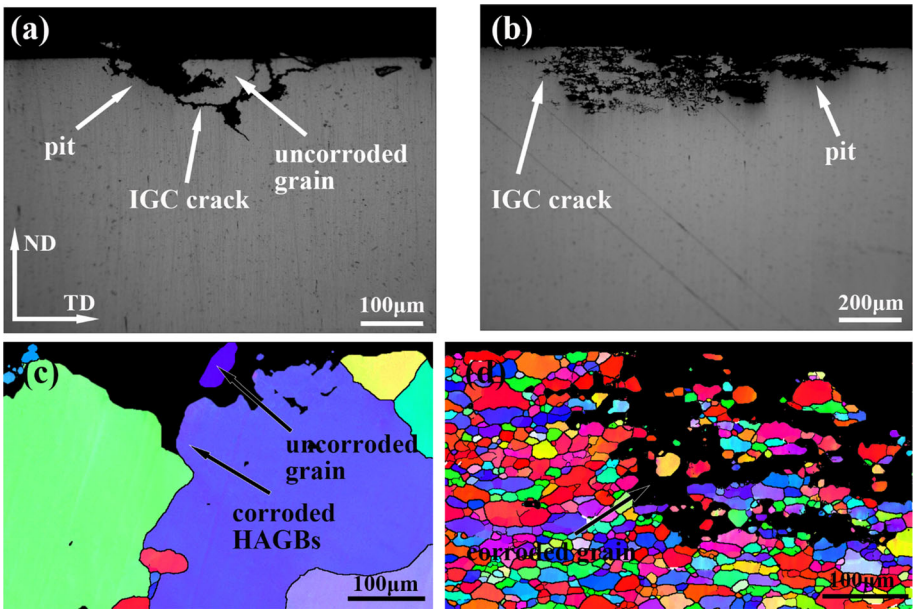

Figure 2 Optical micrographs of the cross sections of **a** the PCG specimen and **b** the PRG specimen after accelerated corrosion test. Corresponding EBSD maps of **a**, **b** are shown in **c**, **d**, respectively.

Table 1 Measured results of accelerated corrosion test

Specimens	Maximum crack depth (μm)	Maximum crack width (μm)	Average crack depth (μm)
PCG specimen	127.5	222.0	34.7 ± 24.7
PRG specimen	233.3	623.3	143.2 ± 47.2

Table 1. The average depth of IGC cracks was obtained by averaging the depth values of all the IGC cracks in specimens. The cracks in PRG specimen were found to be wider and deeper than those in PCG specimen, which indicates that PRG structure is more sensitive to IGC than PCG structure.

EBSD analysis was performed on the areas shown in Fig. 2a, b, as shown in Fig. 2c, d. Due to the low indexing rate, some grains on PCG specimen's surface are invisible in EBSD maps, but in fact they are not corroded, as shown in the optical micrograph. In PCG specimen, only IGC propagating along HAGBs and pitting corrosion were found. The grains on both sides of the corroded HAGBs remain uncorroded. However, except IGC and pitting corrosion, intragranular corrosion was found in PRG specimen, which was indicated by the disappearance of the grains beside some corroded grain boundaries. Also, it should be noticed that the morphology of grain boundaries is almost same to that of IGC cracks for PCG specimen and PRG specimen, which reflects the effect of the grain characteristic on IGC.

The cross sections of the PRG specimens after accelerated corrosion test were also examined with a SEM, and it was found that there are bright particles within IGC cracks and grains interior, as shown in Fig. 3. Trenches were found around those bright particles, which indicates that those particles act as cathodes and cause a dissolution of aluminum matrix. The semi-quantitative analysis on the

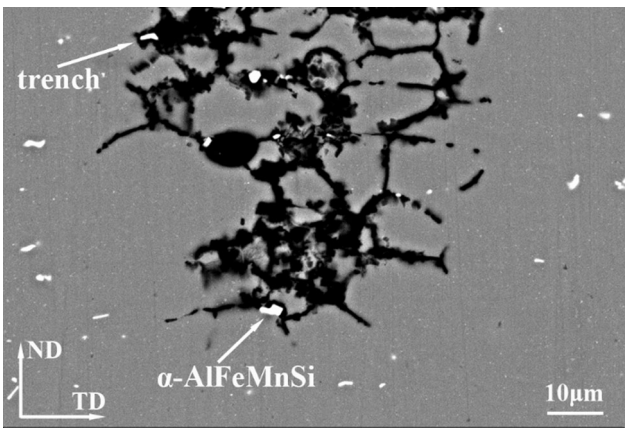

Figure 3 SEM micrograph of the cross section of PRG specimen after accelerated corrosion test.

composition of those particles was performed, and its results reveal that the chemical composition of these particles is about Al 80 at%, Fe 9 at%, Mn 4 at%, Si 7 at% and very few Cu, and hence, these particles are supposed to be primary α-AlFeMnSi intermetallic particles according to their composition, distribution and size. However, this phenomenon was not found in PCG specimen since the IGC cracks are much fewer and shallower; hence, the SEM micrographs of the IGC cracks in PCG specimen are not shown here. It is clear that PCG specimen and PRG specimen show different IGC behaviors, and the IGC of 6005A alloy is affected by AlFeMnSi particles, but more investigation is needed to understand why those differences took place and to reveal the detailed IGC behavior of PCG specimen and PRG specimen.

EIS measurement

The Nyquist diagrams and the Bode diagrams of the PCG specimen and the PRG specimen immersed in a naturally aerated acidified sodium chloride solution are shown in Fig. 4a, b, respectively. The Nyquist diagrams of both specimens consist of a high-frequency capacitive reactance arc, an intermediate-frequency inductive reactance arc and a low-frequency inductive reactance arc. The high-frequency capacitive reactance arc is attributed to interface reactions, especially the oxidation reaction of aluminum matrix [37], and the inductive reactance arc can be attributed to the adsorption of intermediate products on the surface of specimen [38]. In addition, the number of inductive reactance arcs is usually equal to that of the adsorbed species [39]. The shape of the impedance spectrum in Nyquist diagrams indicates a typical active corrosion in both the PCG specimen and PRG specimen immersed in an acidified sodium chloride solution, and two species are absorbed on specimen's surface. It can be supposed that at least two different corrosion reactions take place on specimen's surface and two different species are produced and then absorbed. Apparently, one was Cl^-, but the other remains unclear. Correspondingly, three time constants (the number of the peak and the trough of phase angle) were found in the Bode diagrams of both specimens and they represent the three

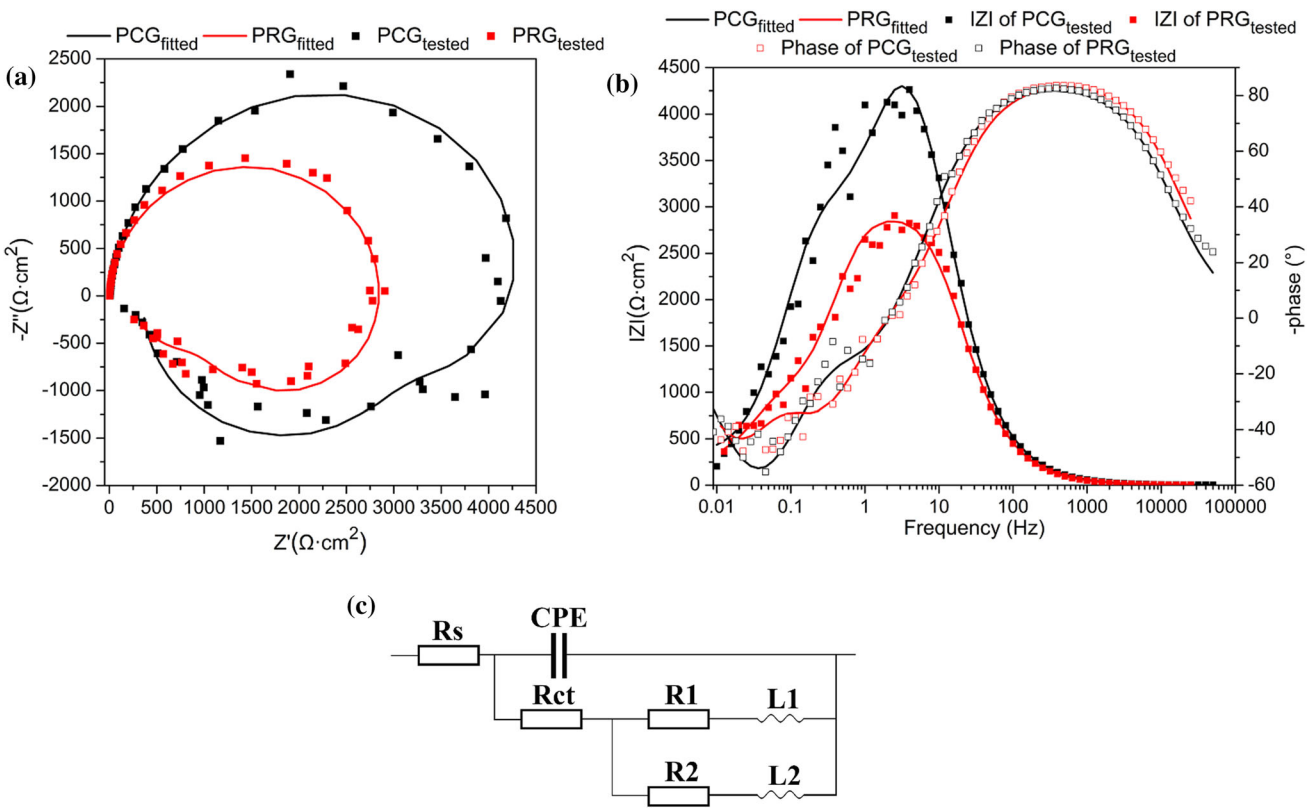

Figure 4 Results of the EIS measurement on the extruded 6005A alloy profile immersed in an acidified sodium chloride solution at open-circuit potential: **a** Nyquist diagram, **b** Bode diagram and **c** equivalent circuit model.

reactance arcs in the Nyquist diagrams, respectively. The high-frequency capacitive reactance arc is represented by a peak with the phase angles approaching − 80°, and two inductive reactance arcs are represented by two troughs with a negative phase angle.

The equivalent circuit model shown in Fig. 4c was used to analyze the impedance diagrams of both PCG specimen and PRG specimen. In this model, R_s is the electrolyte resistance, R_{ct} is the charge transfer resistance, CPE is the constant phase angle element which characterizes the pseudo-double-layer capacitance, and L_1, L_2, R_1 and R_2 are the inductances and the resistances of the adsorbed species. The fitted values are shown in Table 2, where Q and n are the parameters of CPE and characterize the properties of the pseudo-double-layer capacitance. Q is related to the surface properties and the kinds of the electroactive species; n is an exponent ranging from − 1 to 1. When n = 1, 0.5, 0 and − 1, CPE is equivalent to a capacitor, a Warburg element, a resistance and an inductance, respectively. According to the fitted results, n value of CPE was found to be more than 0.94 in both PCG specimen and PRG specimen, which indicates that the deviation between CPE and an ideal capacitance is little. Meanwhile, the Rct of PCG specimen is larger than that of PRG specimen, which indicates that the corrosion rate of PCG specimen is lower and hence the corrosion resistance of PCG specimen is higher than that of PRG specimen. The results of EIS measurement indicate that in an acidified sodium chloride solution, PCG specimen and PRG specimen show the same corrosion mechanism that two different corrosion reactions take place on specimen's surface within the first half hour of immersion, but PCG specimen was more resistant to corrosion than PRG specimen.

Quasi in situ examination of corrosion process

A more detailed mechanism about the IGC of extruded 6005A alloy profile can be drawn from the quasi in situ examination results, as shown in Fig. 5. Before specimens were corroded, bright and coarse particles, which are supposed to be α-AlFeMnSi intermetallic particles, were found in both PCG specimen and PRG specimen. However, it seems that these particles in PRG specimen have a larger average size, higher area fraction and a different distribution than those in PCG specimen. After specimens were corroded for 0.5 h, a few IGC cracks were found on the surface of specimens and some primary α-AlFeMnSi intermetallic particles disappear, as shown in Fig. 5c, d. The appearance of IGC cracks in the areas where AlFeMnSi particles are not found may be the effect of grain boundary precipitates. However, the disappearance of AlFeMnSi particles is unexpected and it needs to be noticed that the disappearing AlFeMnSi particles only disappear partly. Therefore, it can be concluded that the primary α-AlFeMnSi intermetallic particles on specimen's surface are anodes rather than cathodes and are dissolved in an acidified sodium chloride solution, which leads to the initiation of pitting corrosion. Although this conclusion seems to be contradictory to the results of the accelerated corrosion test and the studies mentioned previously, it can be rationalized because similar phenomenon that AlFeMnSi particles were dealloyed in an acid solution was reported [10, 40]. With the propagation of IGC, the mass transfer process between the bulk solution and the solution within IGC cracks becomes more difficult since IGC cracks (diffusion paths) become longer and narrower and are closed by the formation of corrosion products, which makes the composition of the solution within IGC cracks far more different from that of the bulk solution. Therefore, AlFeMnSi particles show different electrochemical properties with the change of their positions. After specimens were corroded for 2 h, most of the AlFeMnSi particles are dissolved and the previously uncorroded grain boundaries become corroded by either IGC or pitting corrosion, as shown in Fig. 5e, f. After specimens were corroded for 6 h, new IGC cracks are formed on the pits distributing

Table 2 Fitted parameters of EIS measurement

Specimens	R_s (Ω cm^2)	Q (10^{-6} Ω^{-1} cm^{-2} s^{-n})	n	R_{ct} (kΩ cm^2)	R_1 (kΩ cm^2)	L_1 (kH cm^2)	R_2 (kΩ cm^2)	L_2 (kH cm^2)
PCG specimen	4.762	4.225	0.948	4.689	11.300	1.494	0.445	4.698
PRG specimen	3.012	4.364	0.962	2.922	2.577	1.789	0.377	4.609

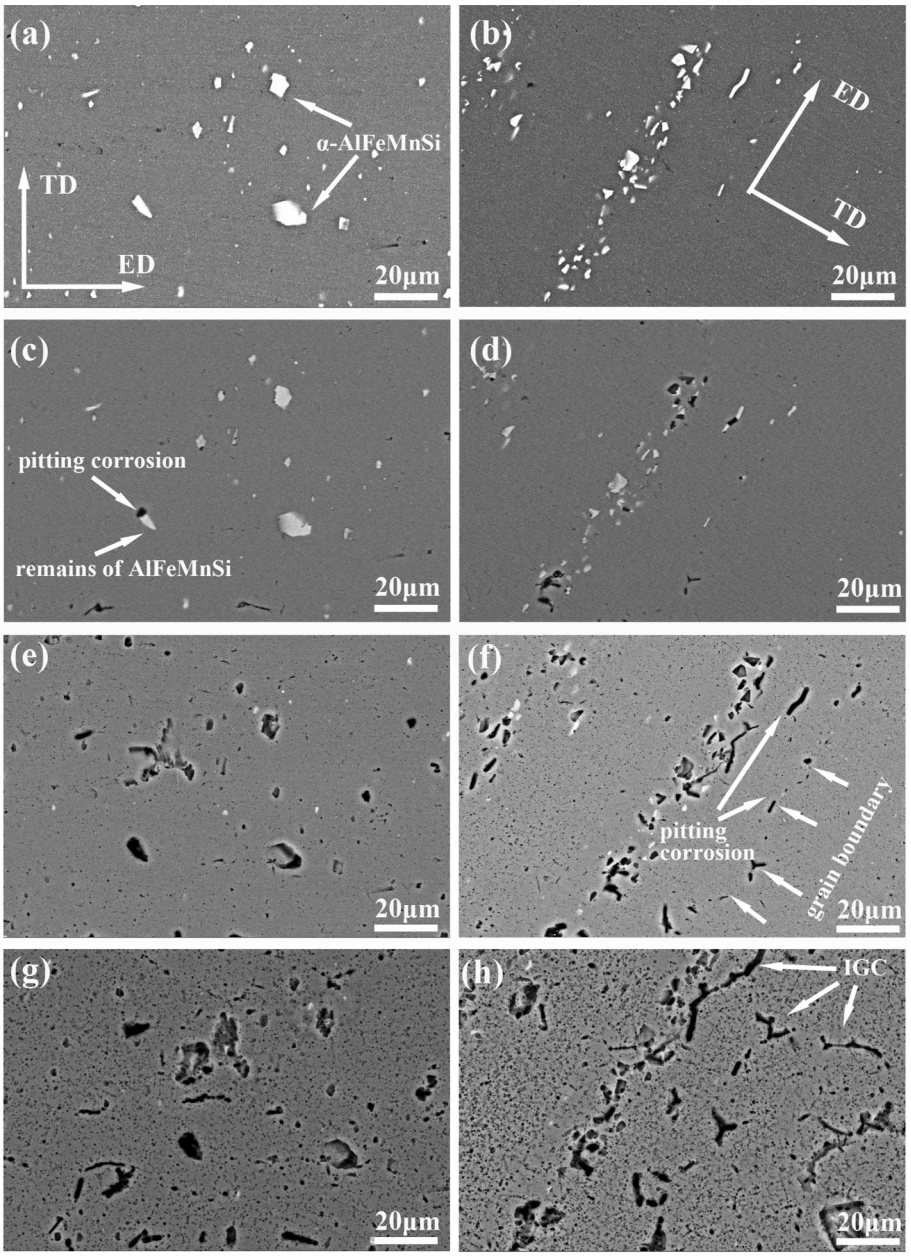

Figure 5 Surface morphological change of the fixed area on PCG specimen and PRG specimen with the increasing in corrosion time. Images **a**, **c**, **e**, **g** and **b**, **d**, **f**, **h** show the surface morphologies of the fixed area on PCG specimen and PRG specimen after specimens were corroded for 0 h, 0.5 h, 2 h, 6 h, respectively.

along grain boundaries and a lot of tiny pits appear on the surface of specimens as shown in Fig. 5g, h, which indicates a change of corrosion mechanism that IGC and foreseeable intragranular corrosion will become the main corrosion reactions.

Eventually, PCG specimen and PRG specimen show two completely different surface morphologies after being immersed for 24 h, as shown in Fig. 6. The pitting corrosion and the IGC in PRG specimen were found to be more severe than those in PCG specimen. On the surface of PCG specimen, most grain boundaries are corroded, but the grains on both sides of grain boundaries are not affected by intragranular corrosion. However, on the surface of PRG specimen, the huge pits surrounded by twisted IGC cracks were found, whose sizes range from hundreds to thousands microns and are much larger than the sizes of AlFeMnSi particles. It was clearly indicated that intragranular corrosion takes place in PRG specimen but not in PCG specimen, and hence, it can be assumed that there are some factors other than AlFeMnSi particles in PRG specimen which causes a transformation of the localized corrosion from IGC and pitting corrosion into intragranular corrosion.

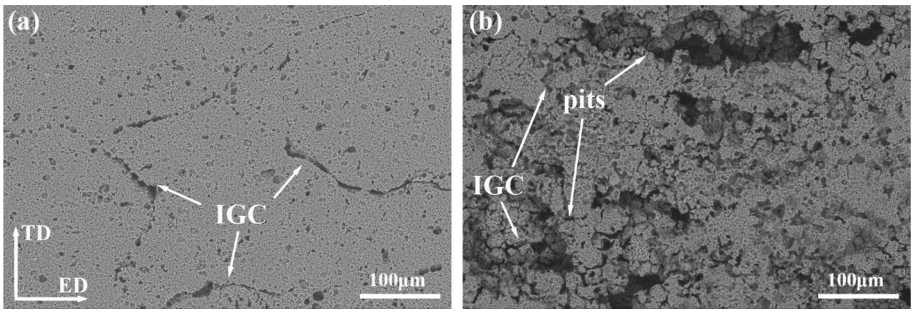

Figure 6 Surface morphologies of **a** PCG specimen and **b** PRG specimen after specimens were corroded for 24 h.

Therefore, the microstructure of both PCG specimen and PRG specimen should be characterized to get a further understanding about the IGC behavior of the extruded 6005A alloy profile with different structures.

Microstructure characterization

EBSD

The EBSD maps of PCG specimen and PRG specimen are shown in Fig. 7a, b, which show two different grain characteristics. The distributions of the equivalent diameters of the grains and the misorientation angles of the grain boundaries in PCG specimen and PRG specimen are shown in Figs. 8 and 9, respectively. In PCG specimen, most grains are completely recrystallized and have quite large sizes, but there were also a few small and partially recrystallized grains. However, in PRG specimen, only a few grains with equiaxed shapes and small sizes were completely recrystallized, and most grains are partially recrystallized. As shown in Fig. 9, the frequency of the HAGBs in PCG specimen is 87.56%, but only 39.57% in PRG specimen, i.e., the frequency of the HAGBs in PCG specimen is higher than that in

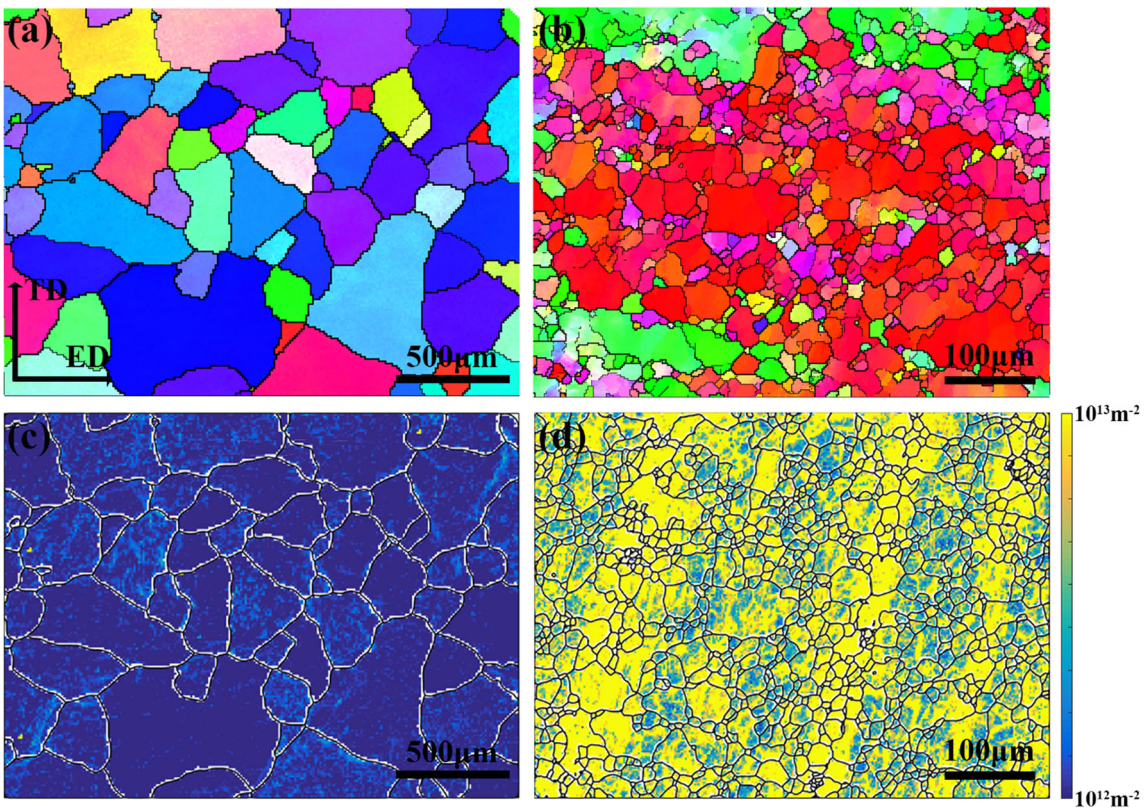

Figure 7 EBSD maps of **a** PCG specimen and **b** PRG specimen. **c**, **d** show the distribution of the dislocation density calculated from the EBSD data of **a**, **b**, respectively.

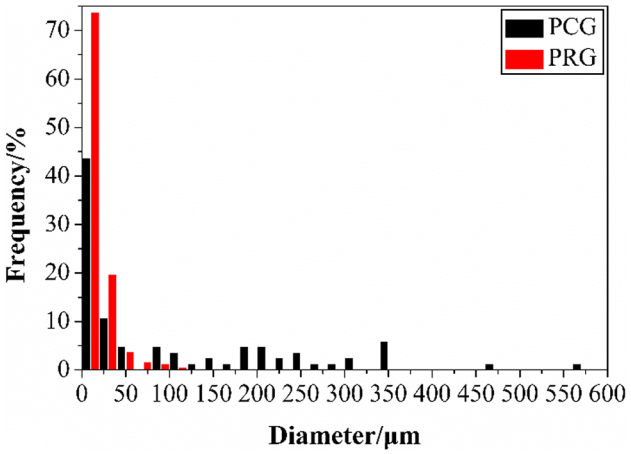

Figure 8 Grain size distribution of PCG specimen and PRG specimen.

PRG specimen. HAGBs were reported to be more sensitive to IGC than LAGBs [34, 41–45], but it does not mean that PCG specimen with a higher frequency of HAGBs is more sensitive to IGC than PRG specimen since the number of the HAGBs exposed to corrosive medium is also determined by the size of grains. Therefore, in spite of the higher frequency of the HAGBs in PCG specimen, the number of the HAGBs exposed to corrosive medium in PCG structure is much less than that in PRG specimen due to the larger size of the grains in PCG specimen [34]. Meanwhile, the HAGBs in PRG specimen were more twisted than those in PCG specimen due to the partial recrystallization and the small size of the grains in PRG specimen. Therefore, the straight IGC cracks in PCG structure and the twisted IGC cracks in PRG structure after specimens were corroded for 24 h were reasonable.

Moreover, recrystallization dramatically decreases dislocation density, which surely has an effect on the IGC behavior of extruded 6005A alloy profile. The contour maps of the geometrically necessary dislocation density in PCG specimen and PRG specimen calculated from EBSD data with the method described in the literature [46] are shown in Fig. 7c, d. It was found that the dislocation density in PRG specimen is almost one order higher than that in PCG specimen. Dislocation is supposed to be the channel of atomic diffusion which promotes the rupture of passive film. Meanwhile, high dislocation density means more stored energy, which increases the thermodynamic driving force for corrosion. Therefore, the high dislocation density in PRG specimen should be responsible for the appearance of intragranular corrosion.

SEM

It was previously mentioned that the distribution, size and the area fraction of AlFeMnSi particles seem to be different in PCG specimen and PRG specimen; hence, they were carefully examined. As shown in Fig. 10, it was found that the area fraction and the average diameter of the AlFeMnSi particles in PCG specimen are 1.291% and 2.703 μm, respectively, but those in PRG specimen are 1.917% and 3.501 μm, respectively. In addition, the distribution of the AlFeMnSi particles in PCG specimen is more uniform than that in PRG specimen where most AlFeMnSi

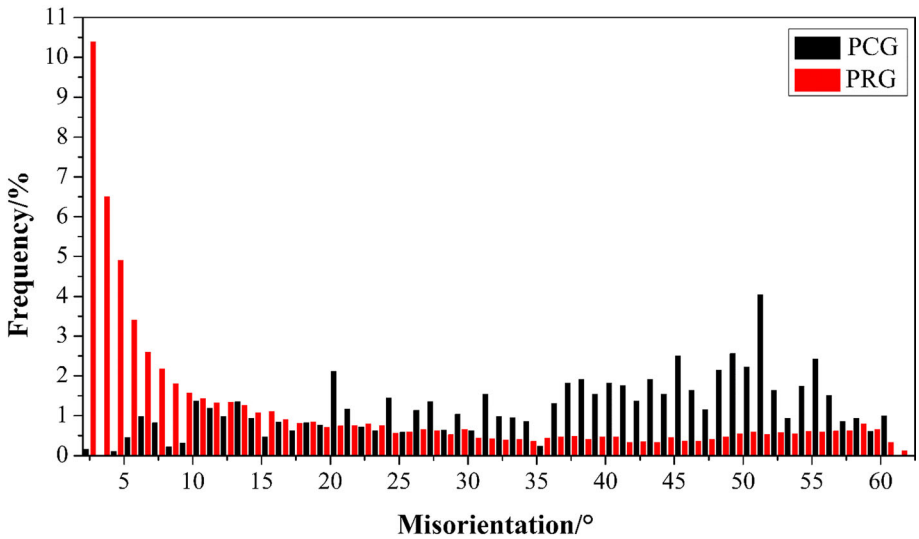

Figure 9 Misorientation angle distribution of PCG specimen and PRG specimen.

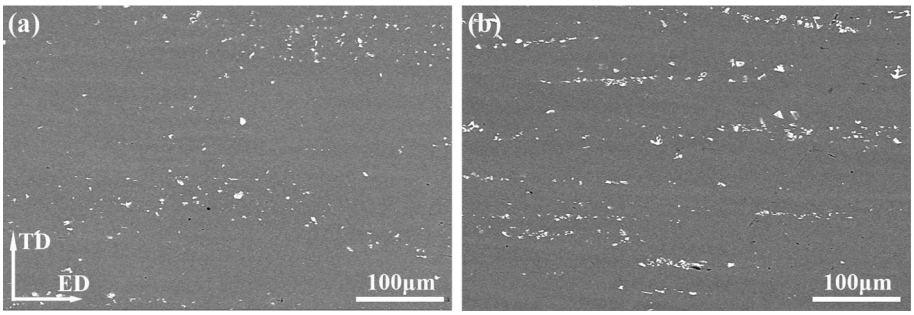

Figure 10 Primary α-AlFeMnSi intermetallic particles in **a** PCG specimen and **b** PRG specimen.

particles are distributed along the extrusion direction. Primary α-AlFeMnSi particles usually exist at grain boundaries; hence in both PCG specimen and PRG specimen, most grain boundaries are decorated with AlFeMnSi particles and IGC propagates from one AlFeMnSi particle to the next. Meanwhile, as more and larger AlFeMnSi particles were found in PRG specimen, more severe pitting corrosion takes place on the surface of PRG specimen, as shown in Fig. 5.

STEM

The grain boundary precipitates of PCG specimen and PRG specimen which were characterized with STEM are shown in Fig. 11a, b, respectively, and all specimens were imaged along the $\langle 001 \rangle_{Al}$ orientation. STEM can clearly characterize the precipitates containing the elements of high atomic number, especially Cu-containing precipitates and Fe-containing precipitates, in 6005A alloy since those precipitates will be represented with a brighter color in STEM images. In both PCG specimen and PRG specimen, grain interior and grain boundaries were found to be decorated with bright precipitates. The composition of those precipitates was found to be about 93.6 at% Al, 2.68 at% Mg, 2.03 at% Si and 1.61 at% Cu by using an EDS, which are supposed to be Q phase precipitates. The precipitates in grain interior were found to be plate-like Q phase precipitates and spherical AlFeMnSi particles, but these phases have little effect on the IGC of alloys. The Q phase grain boundary precipitates with a nobler potential than aluminum matrix are the cathodes in IGC, whose distribution determines the rate of IGC. By comparing the distribution of the Q phase grain boundary precipitates in PCG specimen and PRG specimen, it was found that the distribution of the Q phase precipitates at grain boundary in PRG specimen is more continuous than that in PCG specimen. Therefore, PRG specimen is more sensitive to IGC than PCG specimen as the accelerated corrosion test demonstrated. In addition, no significant difference of the precipitates in grain interior between PCG specimen and PRG specimen was found.

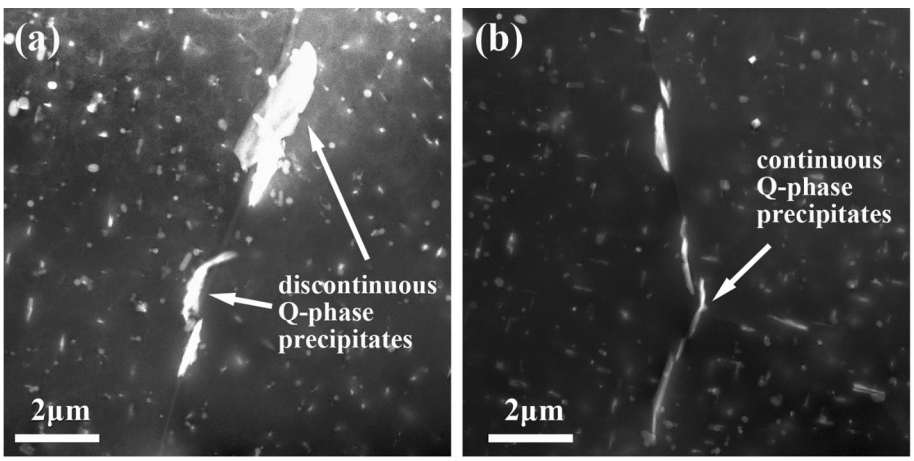

Figure 11 Grain boundary precipitates in **a** PCG specimen and **b** PRG specimen.

Discussion

According to the results of accelerated corrosion test shown in Fig. 2, the IGC resistance of PCG structure is found to be higher than that of PRG structure. Subsequent EIS measurement confirms this conclusion and further reveals that PRG structure has a lower charge transfer resistance and hence a higher corrosion rate than PCG structure as shown in Table 2. Meanwhile, two inductive reactance arcs are found in PCG structure and PRG structure by the EIS measurement as shown in Fig. 4, which indicates the presence of two kinds of corrosion products absorbed on the surface of grains. Quasi in situ examination of corrosion process reveals the origin of these two corrosion products, i.e., the pitting corrosion and the IGC caused by the dissolution of AlFeMnSi particles and aluminum matrix, respectively, as shown in Fig. 5. With the development of corrosion, the AlFeMnSi particles in material interior shown in Fig. 3 are no longer being dissolved, which indicates a transformation of AlFeMnSi particles from anodes into cathodes. In addition, intragranular corrosion only takes place in PRG structure and leads to the formation of huge pits on the specimen's surface with their sizes much more than those of AlFeMnSi particles as shown in Fig. 6.

Although the IGC behaviors of the PCG structure and the PRG structure of extruded 6005A alloys profile in an acidified sodium chloride solution including their corrosion resistances and corrosion processes were revealed, what kinds of microstructural factors such as grain boundary precipitates, grain characteristic and primary α-AlFeMnSi intermetallic particles should be responsible for the different IGC behaviors of PCG structure and PRG structure and which one among them is the most significant are still unsettled. To discuss this, the process of IGC should be divided into two stages. The first stage is the initiation of IGC, and the second stage is the propagation of IGC.

In the first stage, both pitting corrosion and IGC take place on the surface of specimens as shown in Fig. 5. The grain boundary precipitates shown in Fig. 11 are supposed to be the reason of the IGC of some grain boundaries as shown in Fig. 5 since no more other particles have been found in these grain boundaries. Meanwhile, the dissolution of the AlFeMnSi particles on the surface of specimens, as shown in Fig. 5, is supposed to be the reason of pitting corrosion. With the acidification of the solution within pits, pitting corrosion penetrates into the interior of alloy [10, 47] and the grain boundaries beneath specimen's surface are exposed to corrosive medium. Due to the existence of the grain boundary precipitates, more IGC cracks initiate and spread out from the pits. Therefore, the dissolution of AlFeMnSi particles promotes the formation of IGC by increasing the number of the grain boundaries exposed to corrosive medium, which is similar to the effect of decreasing grain size.

In the second stage, which is also the more important stage of IGC, IGC propagates along grain boundaries firstly due to the existence of precipitates at grain boundaries. In this paper, only Q phase precipitates were observed at grain boundaries by the STEM examination, but it does not mean that there were only Q phase precipitates at grain boundaries; in fact, β-phase precipitates and Cu film were very likely to exist at grain boundaries, which has been confirmed by the studies [2, 19–25]. It is well known that the corrosion potential of Q phase, β-phase and Cu film is very different, and hence, it leaves a problem that whether the different precipitates at grain boundaries will lead to the change of the IGC mechanism since it is no doubt that β-phase will become the anode and Q phase and Cu film will become the cathode in the IGC of 6xxx alloys due to their corrosion potential [3, 22, 23]. It is reported that β-phase precipitates are always dissolved prior to other kinds of precipitates and Al matrix due to the lively chemical property of Mg element and their most negative corrosion potential [48].However the dissolution of β-phase precipitates is actually not a complete dissolution [27, 48]. As the migration of Mg element from β-phase precipitates into solution, Si element is remained, which makes β-phase precipitates transformed into Si remnants. In the end, SiO_2·nH_2O deposits are formed on the surface of the Si remnants which act as an additional diffusion barrier hindering the deep propagation of corrosion. By this time, the transformation of β-phase precipitates has been completed, which means the anodes of IGC are no longer β-phase precipitates but turn to be the Al matrix since the existence of the cathodes, i.e., Q phase and Cu film, at grain boundary. Therefore, the existence of β-phase at grain boundary besides the existence of Q phase and Cu film will not change the fact that the Al matrix will be dissolved as the anode in the IGC of 6xxx alloys. However, it is important to

note that although Q phase precipitates act as the cathode throughout the process of IGC, a similar dealloying process will take place on Q phase precipitates, but due to the redeposition of Cu particles upon Q phase precipitates, the role of Q phase precipitates in IGC is not changed [23]. With the dissolution of the Al matrix along the grain boundary, corrosion penetrates into the interior of alloy and due to the change of the composition of the solution within IGC cracks, the AlFeMnSi particles within IGC cracks are transformed into cathodes and promote the propagation of IGC. However, different from grain boundary precipitates, AlFeMnSi particles cannot form the continuous channels for IGC and hence initiate the IGC; they can only become the bridge of IGC that connects grain boundary precipitates because of their discontinuous distribution and low number density at grain boundaries. With the propagation of IGC, the grains containing high dislocation density are exposed to corrosive medium. Due to their poor corrosion resistance, corrosion penetrates into their interior, which means localized corrosion is transformed into intragranular corrosion [18]. The taking place of the transformation of localized corrosion into intragranular corrosion in PRG structure means that the effect of dislocation density plays an important role. No strong correlation between the potential factors, such as the precipitates within grains and the grain orientation, and intragranular corrosion was found in the present paper.

Based on the above discussion, the grain boundary precipitates with a relatively continuous distribution are supposed to be the primary cause of the initiation of IGC because no matter how many grain boundaries are exposed to corrosive medium, if there is no micro-galvanic couples consisting of precipitates and aluminum matrix at grain boundaries, no IGC shall occur. The experimental data of the literature [31] that the overaged Al–Mg–Si–Cu alloy with no obvious grain boundary precipitates was immune to IGC also suggest the conclusion that the effect of grain boundary precipitates on IGC is the most significant. AlFeMnSi particles and grain characteristic have a quite similar effect on increasing the number of grain boundaries exposed to corrosive medium on the initiation stage of IGC, but their effects become different during the propagation of IGC since the role of AlFeMnSi particles and the form of localized corrosion changed.

The above conclusions also explain why the corrosion resistance of PCG specimen and PRG specimen was different. As revealed by the accelerated corrosion test, EIS and the quasi in situ examination of IGC process, PCG specimen is more resistant to pitting corrosion, IGC and intragranular corrosion than PRG specimen. From the previous discussion, it was found that the AlFeMnSi particles on the surface of specimens are dissolved, which leads to the initiation of pitting corrosion. Since the AlFeMnSi particles in PRG specimen are larger and more than those in PCG specimen as shown in Fig. 10, more severe pitting corrosion takes place on the surface of PRG specimen and hence more grain boundaries beneath specimen's surface are exposed to corrosive medium, which reduces the IGC resistance of PRG specimen. Meanwhile, due to the existence of more continuously distributed grain boundaries precipitates shown in Fig. 11, PRG specimen shows a poorer IGC resistance than PCG specimen, which was carefully investigated in an early work [49]. The higher dislocation density remained by partially recrystallization in PRG specimen eventually leads to the taking place of the intragranular corrosion, but in PCG specimen, dislocation density is not high enough to make corrosion penetrating from grain boundaries into grain interior. In a word, in spite of its poor mechanical properties, extruded 6005A profile with PCG structure shows a unique IGC behavior and a high resistance to pitting corrosion, IGC and intragranular corrosion because of its microstructure.

Conclusions

1. The PCG structure of extruded 6005A alloy profile shows a higher corrosion resistance to pitting corrosion, IGC and intragranular corrosion than PRG structure and has a unique IGC behavior that pitting corrosion and subsequent IGC become less severe and are not transformed into intragranular corrosion as they are in PRG structure. The continuity of grain boundary precipitates, the quantity and the size of primary α-AlFeMnSi intermetallic particles and the grain characteristic are found to play an important role in the corrosion of extruded 6005A alloy profile.
2. When extruded 6005A Al–Mg–Si–Cu alloy profile is immersed in an acidified sodium chloride solution, pitting corrosion and IGC take place

on the surface of specimen at first and then pitting corrosion is transformed into IGC. With the propagation of IGC, intragranular corrosion takes place in PRG structure but not in PCG structure.

3. The continuously distributed precipitates at grain boundaries and the high dislocation density in grains are the cause of IGC and intragranular corrosion, respectively. The AlFeMnSi particles on surface are dissolved in an acid environment, which leads to the initiation of pitting corrosion and increases the number of grain boundaries exposed to corrosive medium. With the change of their position, the AlFeMnSi particles within alloy become cathodes and hence the bridge of IGC propagation. Grain characteristic determines the morphology, number and the misorientation angle of grain boundaries and the dislocation density of grains; hence, it affects the IGC behavior of alloy.

Acknowledgements

The authors gratefully acknowledge the financial support of this work by National Natural Science Foundation (Project No. 51474240) and Provincial Science and Technology Major Project of Hunan province (Project No. 2016KG1004).

Compliance with ethical standards

Conflicts of interest The authors declare that they have no conflict of interest to this work.

References

[1] Zhang C, Wang C, Zhang Q, Zhao G, Chen L (2019) Influence of extrusion parameters on microstructure, texture, and second-phase particles in an Al–Mg–Si alloy. J Mater Process Technol 270:323–334

[2] Svenningsen G, Larsen MH, Walmsley JC, Nordlien JH, Nisancioglu K (2006) Effect of artificial aging on intergranular corrosion of extruded AlMgSi alloy with small Cu content. Corros Sci 48:1528–1543

[3] Svenningsen G, Lein JE, Bjorgum A, Nordlien JH, Yu YD, Nisancioglu K (2006) Effect of low copper content and heat treatment on intergranular corrosion of model AlMgSi alloys. Corros Sci 48:226–242

[4] Larsen MH, Walmsley JC, Lunder O, Mathiesen RH, Nisancioglu K (2008) Intergranular corrosion of copper-containing AA6xxx AlMgSi aluminum alloys. J Electrochem Soc 155:C550–C556

[5] Zou Y, Liu Q, Jia ZH, Xing Y, Ding LP, Wang XL (2017) The intergranular corrosion behavior of 6000-series alloys with different Mg/Si and Cu content. Appl Surf Sci 405:489–496

[6] Liang WJ, Rometsch PA, Cao LF, Birbilis N (2013) General aspects related to the corrosion of 6xxx series aluminium alloys: exploring the influence of Mg/Si ratio and Cu. Corros Sci 76:119–128

[7] El-Menshawy K, El-Sayed AWA, El-Bedawy ME, Ahmed HA, El-Raghy SM (2012) Effect of aging time at low aging temperatures on the corrosion of aluminium alloy 6061. Corros Sci 54:167–173

[8] Larsen MH, Walmsley JC, Lunder O, Nisancioglu K (2010) Effect of excess silicon and small copper content on intergranular corrosion of 6000-series aluminium alloys. J Electrochem Soc 157:C61–C68

[9] Kairy SK, Alam T, Rometsch PA, Davies CHJ, Banerjee R, Birbilis N (2016) Understanding the origins of intergranular corrosion in copper-containing Al–Mg–Si alloys. Metall Mater Trans A Phys Metall Mater Sci 47A:985–989

[10] Guillaumin V, Mankowski G (2000) Localized corrosion of 6056 T6 aluminium alloy in chloride media. Corros Sci 42:105–125

[11] Zhang WL, Frankel GS (2003) Transitions between pitting and intergranular corrosion in AA2024. Electrochim Acta 48:1193–1210

[12] Chen MY, Deng YL, Tang JG, Fan ST, Zhang XM (2019) A study of the crystallographic pitting behavior of Al-0.54 Mg-0.66 Si aluminum alloy in acidic chloride solutions. Mater Charact 148:259–265

[13] Zhang XX, Zhou XR, Hashimoto T et al (2017) The influence of grain structure on the corrosion behaviour of 2A97-T3 Al–Cu–Li alloy. Corros Sci 116:14–21

[14] Zhang XX, Zhou XR, Hashimoto T et al (2018) Corrosion behaviour of 2A97-T6 Al–Cu–Li alloy: the influence of non-uniform precipitation. Corros Sci 132:1–8

[15] Luo C, Zhou X, Thompson GE, Hughes AE (2012) Observations of intergranular corrosion in AA2024-T351: the influence of grain stored energy. Corros Sci 61:35–44

[16] Ly R, Hartwig KT, Castaneda H (2018) Effects of strain localization on the corrosion behavior of ultra-fine grained aluminum alloy AA6061. Corros Sci 139:47–57

[17] Guerin M, Alexis J, Andrieu E, Laffont L, Lefebvre W, Odemer G, Blanc C (2016) Identification of the metallurgical parameters explaining the corrosion susceptibility in a 2050 aluminium alloy. Corros Sci 102:291–300

[18] Zhang XX, Jiao YB, Yu Y, Liu B, Hashimoto T, Liu HF, Dong ZH (2019) Intergranular corrosion in AA2024-T3 aluminium alloy: the influence of stored energy and prediction. Corros Sci 155:1–12

[19] Chakrabarti DJ, Laughlin DE (2004) Phase relations and precipitation in Al–Mg–Si alloys with Cu additions. Prog Mater Sci 49:389–410

[20] Kairy SK, Rometsch PA, Diao K, Nie JF, Davies CHJ, Birbilis N (2016) Exploring the electrochemistry of 6xxx series aluminium alloys as a function of Si to Mg ratio, Cu content, ageing conditions and microstructure. Electrochim Acta 190:92–103

[21] Kairy SK, Birbilis N, Rometsch PA, Davies CHJ (2015) The influence of copper additions and aging on the microstructure and metastable pitting of Al–Mg–Si alloys. Corrosion 71:1304–1307

[22] Kairy SK, Rometsch PA, Davies C, Birbilis N (2017) On the intergranular corrosion and hardness evolution of 6xxx series Al-alloys as a function of Si: Mg ratio, Cu content and ageing condition. Corrosion 73:1280–1295

[23] Kairy SK, Rometsch P, Davies C, Birbilis N (2017) On the electrochemical and quasi in situ corrosion response of the Q-phase (AlxCuyMgzSiw) intermetallic particle in 6xxx series Al-alloys. Corrosion 73:87–99

[24] Svenningsen G, Larsen MH, Nordlien JH, Nisancioglu K (2006) Effect of high temperature heat treatment on intergranular corrosion of AlMgSi(Cu) model alloy. Corros Sci 48:258–272

[25] Svenningsen G, Larsen MH, Nordlien JH, Nisancioglu K (2006) Effect of thermomechanical history on intergranular corrosion of extruded AlMgSi(Cu) model alloy. Corros Sci 48:3969–3987

[26] Remoe MS, Marthinsen K, Westermann I, Pedersen KT, Royset J, Marioara C (2017) The effect of alloying elements on the ductility of Al–Mg–Si alloys. Mater Sci Eng A Struct Mater Prop Microstruct Process 693:60–72

[27] Yasakau KA, Zheludkevich ML, Lamaka SV, Ferreira MGS (2007) Role of intermetallic phases in localized corrosion of AA5083. Electrochim Acta 52:7651–7659

[28] Birbilis N, Buchheit RG (2005) Electrochemical characteristics of intermetallic phases in aluminum alloys—an experimental survey and discussion. J Electrochem Soc 152:B140–B151

[29] Zander D, Schnatterer C, Altenbach C, Chaineux V (2015) Microstructural impact on intergranular corrosion and the mechanical properties of industrial drawn 6056 aluminum wires. Mater Des 83:49–59

[30] Kumari S, Wenner S, Walmsley JC, Lunder O, Nisancioglu K (2019) Progress in understanding initiation of intergranular corrosion on AA6005 aluminum alloy with low copper content. J Electrochem Soc 166:C3114–C3123

[31] Li H, Zhao PP, Wang ZX, Mao QZ, Fang BJ, Song RG, Zheng ZG (2016) The intergranular corrosion susceptibility of a heavily overaged Al–Mg–Si–Cu alloy. Corros Sci 107:113–122

[32] De Pari L, Misiolek WZ (2008) Theoretical predictions and experimental verification of surface grain structure evolution for AA6061 during hot rolling. Acta Mater 56:6174–6185

[33] Minoda T, Yoshida H (2002) Effect of grain boundary characteristics on intergranular corrosion resistance of 6061 aluminum alloy extrusion. Metall Mater Trans A Phys Metall Mater Sci 33:2891–2898

[34] Wloka J, Hack T, Virtanen S (2007) Influence of temper and surface condition on the exfoliation behaviour of high strength Al–Zn–Mg–Cu alloys. Corros Sci 49:1437–1449

[35] Ralston KD, Birbilis N, Davies CHJ (2010) Revealing the relationship between grain size and corrosion rate of metals. Scr Mater 63:1201–1204

[36] Zhang XX, Zhou XR, Nilsson JO, Dong ZH, Cai CR (2018) Corrosion behaviour of AA6082 Al–Mg–Si alloy extrusion: recrystallized and non-recrystallized structures. Corros Sci 144:163–171

[37] Khireche S, Boughrara D, Kadri A, Hamadou L, Benbrahim N (2014) Corrosion mechanism of Al, Al–Zn and Al–Zn–Sn alloys in 3 wt.% NaCl solution. Corros Sci 87:504–516

[38] Cabot PL, Garrido JA, Perez E, Moreira AH, Sumodjo PTA, Proud W (1995) Eis study of heat-treated Al–Zn–Mg alloys in the passive and transpassive potential regions. Electrochim Acta 40:447–454

[39] Chen WC, Wen TC, Gopalan A (2002) Negative capacitance for polyaniline: an analysis via electrochemical impedance spectroscopy. Synth Met 128:179–189

[40] Suter T, Alkire RC (2001) Microelectrochemical studies of pit initiation at single inclusions in Al 2024-T3. J Electrochem Soc 148:B36–B42

[41] Tan L, Allen TR (2010) Effect of thermomechanical treatment on the corrosion of AA5083. Corros Sci 52:548–554

[42] Yang WC, Ji SX, Li Z, Wang MP (2015) Grain boundary precipitation induced by grain crystallographic misorientations in an extruded Al–Mg–Si–Cu alloy. J Alloy Compd 624:27–30

[43] Liu Y, Zhou X, Thompson GE, Hashimoto T, Scamans GM, Afseth A (2007) Precipitation in an AA6111 aluminium alloy and cosmetic corrosion. Acta Mater 55:353–360

[44] Zhang RF, Qiu Y, Qi YS, Birbilis N (2018) A closer inspection of a grain boundary immune to intergranular corrosion in a sensitised Al–Mg alloy. Corros Sci 133:1–5

[45] Wang ZX, Zhu F, Zheng K et al (2018) Effect of the thickness reduction on intergranular corrosion in an under-

aged Al–Mg–Si–Cu alloy during cold-rolling. Corros Sci 142:201–212

[46] Pantleon W (2008) Resolving the geometrically necessary dislocation content by conventional electron backscattering diffraction. Scr Mater 58:994–997

[47] Soltis J (2015) Passivity breakdown, pit initiation and propagation of pits in metallic materials—review. Corros Sci 90:5–22

[48] Eckermann F, Suter T, Uggowitzer P, Afseth A, Schmutz P (2008) The influence of MgSi particle reactivity and dissolution processes on corrosion in Al–Mg–Si alloys. Electrochim Acta 54:844–855

[49] Shen PY, Tang JG, Ye LY, Duan CX, Den YL (6005A) Effect of microstructure heterogeneity on intergranular corrosion susceptibility of Al-alloy 6005A. Chin J Mater Res 32:751–758 **(in Chinese)**